รายงานการวิจัย

การวิเคราะห์การลดทอนสัญญาณรบกวนในการถ่ายภาพคลื่นเสียงความถี่สูง

Analysis of Noise Reduction in Medical Ultrasound Imaging

ผลงานวิจัยเป็นความรับผิดชอบของหัวหน้าโครงการวิจัยแต่เพียงผู้เดียว

รหัสโครงการ SUT1-103-54-12-27

รายงานการวิจัย

การวิเคราะห์การลดทอนสัญญาณรบกวนในการถ่ายภาพคลื่นเสียงความถี่สูง
Analysis of Noise Reduction in Medical Ultrasound Imaging

คณะผู้วิจัย

หัวหน้าโครงการ
ผศ. ดร. เจษฎา ตัณฑนุช
สาขาวิชาคณิตศาสตร์
สำนักวิชาวิทยาศาสตร์
มหาวิทยาลัยเทคโนโลยีสุรนารี
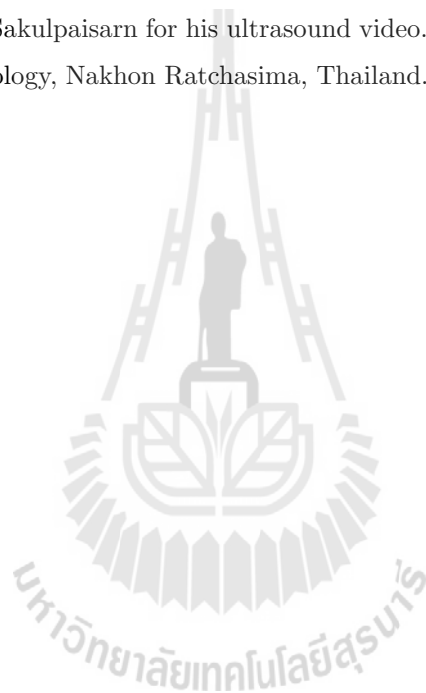
ผู้ร่วมวิจัย

Asst. Prof Dr. Eckart Schulz

กันยายน 2558

Acknowledgements

บทคัดย่อ

งานวิจัยชิ้นนี้ ได้พัฒนาแบบจำลองทางคณิตศาสตร์แบบการแปรผันสำหรับการลดสัญญาณรบกวน แบบสเปกเคิลในภาพถ่ายคลื่นเสียงความถี่สูง โดยมีสมมติฐานว่าสัญญาณรบกวนแบบสเปกเคิลมี รูปแบบการแจกแจงแบบเรย์ลี แบบจำลองทางคณิตศาสตร์ดังกล่าวนำไปสู่การหาค่าน้อยสุดของ ฟังก์ชันนัลบนปริภูมิของฟังก์ชันของการแปรผันอย่างมีขอบเขต ฟังก์ชันนัลดังกล่าวประกอบด้วย พจน์ของพลังงานและพจน์ของความถูกต้องของข้อมูล ซึ่งได้มาจากการแจกแจงแบบเรย์ลี งานวิจัย ชิ้นนี้แสดงให้เห็นว่าค่าน้อยสุดของฟังก์ชันนัลมีอยู่จริง และมีอยู่เพียงหนึ่งเดียวภายใต้เงื่อนไขเพิ่มเติม บางประการ ผลเฉลยของสมการออยเลอร์-ลากรานจ์ของแบบจำลองทางคณิตศาสตร์ที่ได้ ถูก ประมาณโดยวิธีเกรเดียนต์เดสเซนต์

ในส่วนของการทวนสอบความถูกต้องของแบบจำลอง ภาพที่มีลักษณะเป็นแบบรูปและภาพ ของเลนนาได้ถูกนำมาใช้เป็นตัวอย่างการทดสอบ และผลการทำสอบได้ทำการเปรียบเทียบ สหสัมพันธ์ระหว่างภาพที่มีสัญญาณรบกวนกับภาพต้นแบบ และภาพที่ถูกบูรณะโดยวิธีต่าง ๆ กับ ภาพต้นแบบ ผลการศึกษาพบว่าแบบจำลองที่ได้สามารถลดสัญญาณรบกวนจากภาพที่ใช้ทำการ ทดสอบและวีดิทัศน์ของภาพถ่ายคลื่นเสียงความถี่สูง นอกจากนี้ได้เปรียบเทียบสมรรถนะของการลด สัญญาณรบกวนโดยแบบจำลองที่ได้กับการลดสัญญาณรบกวนโดยแบบจำลองทางคณิตศาสตร์แบบ การแปรผันอื่น ๆ อีกด้วย

Abstract

A variational model for the reduction of speckle noise in ultrasound images is developed, which assumes that speckle noise follows a Rayleigh distribution. The model leads to a functional on the space of functions of bounded variation to be minimized. This functional consists of an energy term and a data-fidelity term derived from the Rayleigh distribution. It is shown that minimizers of the functional exist and, under some additional assumptions, are unique. The solution of the resulting Euler-Lagrange equation is then approximated by the gradient descent method.

For the purpose of verification of the model, a pattern image as well as the Lenna image are used as sample images, and the correlations between the noisy, respectively the reconstructed images and the original ones are compared. It is found that the model can be used successfully to remove noise from images and ultrasound videos. Finally, the performance of this new model is compared with that of some of the variational denoising models described in the literature, by means of the sample images.

Contents

List of Tables

List of Figures

Chapter 1

Introduction

1.1   Background and Rationale

Ultrasound imaging is a widely used tool in the practice of medicine, as it provides low cost, non-invasive and real-time images which may help in diagnosis and therapy. However, the raw images are severely degraded by noise, mainly in the form of speckle noise, and substantial processing is required to remove the noise. Thus, image denoising is an important topic in ultrasound imaging which continues to attract broad research interest in the image processing community at large.

Since speckle noise is of high-frequency nature, low-pass filters may be employed for noise reduction. By their nature, however, such filters tend to blur the images. Better outcomes can be obtained with a class of denoising methods which involve the smoothing of an image by employing local averages. These include the Lee filter [17], the Frost filter [8] and the Kuan filter [15]. More recently, a variety of wavelet-based methods has been used to remove the high-frequency speckle noise [6, 11, 21]. In [18], an enhanced image was obtained as the steady-state solution of a diffusion equation, with the noisy image as its initial condition. Several publications, including [14] have improved on this method, by adding a data-fidelity term to the equation.

In the variational model of [19], the image denoising problem was cast in the form of a convex optimization problem: Find the minimizer u of the functional

$$E(u) = \int_\Omega |\nabla u| + J(u, f)$$

where f is the noisy image, u the desired denoised image, ∇u denotes the gradient, and $J(u, f)$ is a data-fidelity term. The particular fidelity term chosen in [19] is simply the mean-square norm,

$$J(u, f) = \int_\Omega (u - f)^2$$

which is a reasonable choice for additive Gaussian noise. By the method of calculus of variations, the minimizer u can be found as the solution of an Euler-Lagrange equation. In [16] this fidelity term was modified to account for additive noise of Poisson type.

Most models in the literature represent speckle noise as multiplicative noise. The data fidelity term chosen in the variational model of [1] corresponds to speckle noise appearing in small aperture radio (SAR) radar imaging, involving an exponential distribution. In contrast, noise in ultrasound imaging usually involves the Rayleigh distribution [3].

1.2 Research Objectives

The objective of this project was as follows:

1. Develop a mathematical model for image denoising using the variational method introduced in [19], under the specific assumption that pixel brightness involves the Rayleigh distribution.

2. Derive the data-fidelity term which corresponds to this distribution and prove the existence and uniqueness of minimizers.

3. Formulate and solve the corresponding Euler-Lagrange equation numerically, and show by means of standard sample images that this method can be used for image denoising.

1.3 Scope and Limitations

There are a great variety of ultrasound imaging noise reduction techniques available in the literature, most of which do not employ the variational method. Furthermore, even though it is commonly assumed [3] that ultrasound image noise involves the Rayleigh distribution, it is nevertheless reasonable to speculate that other distributions might be better suited for modeling such noise. This research is limited to considering only the variational method and the Rayleigh distribution.

1.4 Benefits from the Research

While focused on ultrasound imaging, this project adds to the general knowledge of image enhancement techniques. It thus may be of use to the community of engineers and scientists who are working with the implementation of noise reduction technologies.

1.5 Outline

This report is organized as follows. In Chapter 2 the model of ultrasound speckle noise used herein and the various denoising models based on [19] are reviewed, and then the proposed variational denoising model for ultrasound speckle noise is developed. Chapter 3 is used to discuss this model mathematically, and to prove the existence and uniqueness of minimizers for this model in the space of functions of bounded variation. Chapter 4 discusses the numerical solution of some samples images, and compares them with the solutions obtained by some other data-fidelity terms.

Chapter 2

Development of the Model

In this chapter we review the derivation of two models for ultrasound speckle noise, one which yields the Rayleigh distribution, and another one which yields the Rician distribution. We then review the variational models for noise reduction in images available in the literature. Finally, we develop our variational model for speckle noise reduction in ultrasound images which employs the Rayleigh probability distribution.

2.1 Speckle Noise

We begin with a brief review of the representation of signals by phasors.

2.1.1 Signals and Phasors

Addition of signals

Let

$$f_k(t) = a_k \cos(\omega t - \theta_k)$$

($\omega = 2\pi F_o$, $0 \leq \theta_k < 2\pi$, $a_k \geq 0$, $k = 1, \ldots, N$) be a finite collection of signals of identical frequency F_o with phase shifts θ_k each. By a trigonometric identity each signal can be expressed as a linear combination,

$$f_k(t) = a_k \left[\cos\theta_k \cos(\omega t) + \sin\theta_k \sin(\omega t) \right].$$

Thus, the sum of the N signals is

$$\sum_{k=1}^{N} f_k(t) = \left[\sum_{k=1}^{N} a_k \cos\theta_k \right] \cos(\omega t) + \left[\sum_{k=1}^{N} a_k \sin\theta_k \right] \sin(\omega t). \tag{2.1}$$

This linear combination is easily expressed as a single signal,

$$a \cos(\omega t - \theta), \tag{2.2}$$

that is, as

$$\sum_{k=1}^{N} f_k(t) = a\left[\cos\theta\cos(\omega t) + \sin\theta\sin(\omega t)\right]. \tag{2.3}$$

In fact, comparing (2.1) with (2.3) we obtain

$$a\cos\theta = \sum_{k=1}^{N} a_k\cos\theta_k \tag{2.4}$$

$$a\sin\theta = \sum_{k=1}^{N} a_k\sin\theta_k. \tag{2.5}$$

Squaring and adding both equations gives

$$a^2 = \sum_{k=1}^{N} a_k^2 + 2\sum_{i=1}^{N}\sum_{k<i} a_i a_k\left[\cos\theta_i\cos\theta_k + \sin\theta_i\sin\theta_k\right]$$

$$= \sum_{k=1}^{N} a_k^2 + 2\sum_{i=1}^{N}\sum_{k<i} a_i a_k\cos(\theta_k - \theta_i)$$

so that

$$a = \sqrt{\sum_{k=1}^{N} a_k^2 + 2\sum_{i=1}^{N}\sum_{k<i} a_i a_k\cos(\theta_k - \theta_i)}.$$

On the other hand, dividing the two equations yields

$$\tan\theta = \frac{\sum_{k=1}^{N} a_k\sin\theta_k}{\sum_{k=1}^{N} a_k\cos\theta_k}$$

which, together with the signs of the right-hand sides of (2.4) and (2.5), uniquely determines the value of θ.

The exponential representation

It is standard practice to express signals of form (2.2) in complex exponential form: Given a fixed frequency F_o, let us set

$$X = \left\{\, f(t) = a\cos(\omega t - \theta)\,:\, a \geq 0,\, 0 \leq \theta < 2\pi \,\right\}$$

$$= \left\{\, f(t) = a\cos(\omega t - \theta)\,:\, a \in \mathbb{R},\, 0 \leq \theta < \pi \,\right\}$$

$(\omega = 2\pi F_o)$, the vector space of all periodic signals of frequency F_o, and

$$Y = \left\{\, g(t) = ce^{-j\omega t}\,:\, c \in \mathbb{C} \,\right\},$$

the space of all complex signals of frequency F_o. Clearly, the map

$$\Phi : f(t) = a\cos(\omega t - \theta) \quad\mapsto\quad g(t) = ae^{-j(\omega t - \theta)} \qquad (a \geq 0,\ 0 \leq \theta < 2\pi)$$

is a bijection of X onto Y. In fact, surjectivity follows from the polar representation of every complex number c, $c = ae^{j\theta}$ where $a \geq 0$ and $0 \leq \theta < 2\pi$. On the other hand, injectivity follows from the fact that $f(t) = \mathfrak{Re}(g(t))$.

We observe that Φ is linear: Homogeneity of Φ is obvious. On the other hand, applying (2.1)–(2.5) with $N = 2$ we obtain

$$
\begin{aligned}
\Phi\big(f_1(t) + f_2(t) \big) = \Phi\big(a \cos (\omega t - \theta) \big) &= a e^{j\theta} e^{-j\omega t} \\
&= [\, a \cos\theta + j a \sin\theta \,] e^{-j\omega t} \\
&= [\, (a_1 \cos\theta_1 + a_2 \cos\theta_2) + j(a_1 \sin\theta_1 + a_2 \sin\theta_2) \,] e^{-j\omega t} \\
&= a_1 [\, \cos\theta_1 + j \sin\theta_1 \,] e^{-j\omega t} + a_2 [\, \cos\theta_2 + j \sin\theta_2 \,] e^{-j\omega t} \\
&= a_1 e^{j\theta_1} e^{-j\omega t} + a_2 e^{j\theta_2} e^{-j\omega t} = \Phi\,(\, f_1(t)\,) + \Phi\,(\, f_2(t)\,)
\end{aligned}
$$

which shows that Φ is additive.

Since all signals $f(t) \in X$ have the same frequency, the factor $a e^{j\theta}$ (determined by the amplitude a and the phase shift θ) uniquely determines $f(t)$; it is called a *phasor*. By linearity of Φ, forming linear combinations of signals in X corresponds to forming linear combinations of their phasors. Thus, one may work with phasors instead of the signals themselves.

2.1.2 Models for Ultrasound Images and Speckle Noise

Let us first give a brief and simplified overview over the principles of ultrasound imaging. A transmitter (called a transducer as it converts an electric wave to a sound wave) emits a short pulse of a unidirectional ultrasound wave. Whenever the pulse encounters a change of acoustic impedance due to a boundary (also called an interface) between two objects, a small fraction of the pulse is reflected back to the transducer, which now acts as a detector and converts the sound wave back to an electric wave. (which is also called a transducer as it converts sound waves to electric waves). A single emitted pulse may result in several returning pulses, depending on the number of interfaces along its path. The time-delay between the emission of a pulse and the arrival of a reflection corresponds to the distance of the corresponding interface from the transducer, while the amplitude of each reflected pulse corresponds to the change of acoustic impedance at that interface.

One distinguishes between two type of reflections. *Specular reflection* occurs at interfaces which are smooth and significantly larger than the wavelength of the ultrasound. Here, a fraction of the wave is reflected back at an angle opposite to the incident angle (with respect to the normal to the interface). Thus, if the incident angle is sufficiently small, then the reflected wave will appear at the detector. *Nonspecular reflection* occurs when the interface is rough and/or has diameter smaller than the wavelength. Here the wave is reflected into all directions, and thus only a small fraction of the reflected wave will arrive at the detector, resulting in low amplitudes. It has been reported that nonspecular reflection carries more weight in medical ultrasound imaging than specular reflection [12].

In order to be able to distinguish between different returning pulses, the line along which the signal travels is modeled to be split into small *resolution cells*, which must be considered long

enough so that the returning pulses from two adjacent cells don't overlap, and which have the cross-sectional width and height of the ultrasound beam. The result of the ultrasound scan can now be represented graphically in several ways, the most common of which is a *B-scan* which will be used here. In a B-scan the pulse returning from each resolution cell is represented as a pixel in a one-dimensional image whose brightness is determined by the amplitude of the return pulse.

Based on these concepts, we now review the derivation of two models for noise in ultrasound images. While there are a variety of additional phenomena which may affect the signal at the detector and lead to noise, such as refraction, diffraction, attenuation by absorption and beam-widening, we will only consider the above two types of reflections in the construction of the models.

Model I: Random reflections leading to the Rayleigh distribution

This is the model presented in [3] and assumes that reflections are non specular. Consider one resolution cell of the ultrasound scanner. Since the dimensions of this cell are assumed to be by orders of magnitude larger than the reflecting interfaces, in this model we think of the cell as composed of a very large number of very small scatterers of equal size. Since different scatterers have different distances from the transmitter/detector, the reflections from the various scatterers will then arrive back at the detector with different phase shifts. Thus, the reflections are best expressed as phasors, in the form $a_k e^{j\theta_k}$, $k = 1, \ldots, N$.

Now suppose a signal of amplitude a is emitted from the transmitter, and reaches a resolution cell. Since the energy of this signal is proportional to a^2 (to be precise, the energy over one period T is

$$\mathcal{E} = \int_0^T |f(t)|^2 \, dt = ca^2 \qquad \text{where} \quad c = \int_0^T \cos^2(\omega t) \, dt = \frac{T}{2}$$

with $T = 1/F_o$), then each scatterer will receive a signal of energy ca^2/N, that is of amplitude $a/\sqrt{N}$. The scatterer now reflects a fraction of this signal in form of a phasor

$$\frac{a_k}{\sqrt{N}} e^{j\theta_k},$$

where the ratio a_k/a signifies what fraction of the incoming wave, in terms of amplitude, is being reflected by the scatterer. Furthermore, the angle θ_k denotes the phase shift with which the reflected wave arrives at the detector. The return signals from all the scatterers will thus combine to a phasor

$$\tilde{a}e^{j\theta} = \frac{1}{\sqrt{N}} \sum_{k=1}^{N} a_k e^{j\theta_k} \tag{2.6}$$

at the detector.

Since reflection is nonspecular and caused by rough surfaces, it is reasonable to assume that the values of a_k and θ_k at each cell are actually random variables, which we denote by A_k and Θ_k, respectively. Hence, $\tilde{a}$ and θ are also assumed to be random variables A and Θ, respectively, so

that (2.6) becomes

$$Ae^{j\Theta} = \frac{1}{\sqrt{N}} \sum_{k=1}^{N} A_k e^{j\Theta_k}. \tag{2.7}$$

Following [9], we make the following assumptions:

1. The amplitude A_k and phase Θ_k of the k-th phasor are independent of each other, and independent of the amplitudes A_i and Θ_i of the other phasors. (That is, $A_1, \ldots, A_n$ and $\Theta_1, \ldots, \Theta_n$ are all independent random variables.)

2. The amplitudes A_k are all identically distributed with mean μ and second moment ρ. This is a reasonable assumption, because all scatterers in the resolution cell are assumed to be of equal size.

3. The phases Θ_k are uniformly distributed in $[0, 2\pi)$. This again is a reasonable assumption as the scatterers in the resolution cell are assumed to be uniformly distributed over the cell.

Let us split the phasor of the return signal into real and imaginary parts,

$$\mathfrak{r} := \mathfrak{Re}(Ae^{j\Theta}) = \frac{1}{\sqrt{N}} \sum_{k=1}^{N} A_k \cos \Theta_k$$

$$\mathfrak{i} := \Im(Ae^{j\Theta}) = \frac{1}{\sqrt{N}} \sum_{k=1}^{N} A_k \sin \Theta_k.$$

It is shown in [9] that, by means of the Central Limit Theorem, $\mathfrak{r}$ and $\mathfrak{i}$ will approach independent Gaussian random variables with means zero and common second moment $\rho/2$ as $N \to \infty$. We may thus assume that the phasor of reflected signal is a random variable of the form

$$Ae^{j\Theta} = [A\cos\Theta + jA\sin\Theta] = [\mathfrak{r} + j\,\mathfrak{i}]$$

where $\mathfrak{r}$ and $\mathfrak{i}$ are independent $\mathcal{N}(0, \sigma^2)$ random variables, that is, they have density functions

$$p_{\mathfrak{r}}(x) = \frac{1}{\sqrt{2\pi}\sigma}e^{-x^2/2\sigma^2} \qquad \text{and} \qquad p_{\mathfrak{i}}(y) = \frac{1}{\sqrt{2\pi}\sigma}e^{-y^2/2\sigma^2},$$

respectively, with $\sigma^2 = \rho/2$. Since the two random variables are independent, their joint distribution is the product of their individual distributions,

$$p_{\mathfrak{r},\mathfrak{i}}(x, y) = p_{\mathfrak{r}}(x)p_{\mathfrak{i}}(y) = \frac{1}{2\pi\sigma^2}e^{-(x^2+y^2)/2\sigma^2}.$$

Now as signals are expressed as phasors, we switch back to polar coordinates, $(x, y) = x + jy = re^{j\varphi}$ and obtain the probability density function of the phasor $Ae^{j\Theta}$,

$$p_{A,\Theta}(r, \varphi) = \frac{r}{2\pi\sigma^2}e^{-r^2/2\sigma^2} \qquad\qquad (r \geq 0, \ 0 \leq \varphi < 2\pi).$$

That is, the probability that $a_1 \leq A \leq a_2$ and $\theta_1 \leq \Theta \leq \theta_2$ is

$$\int_{a_1}^{a_2} \int_{\theta_1}^{\theta_2} \frac{r}{2\pi\sigma^2}e^{-r^2/2\sigma^2} \, d\varphi \, dr.$$

Now the detector measures the amplitude A only, which has the marginal probability density

$$p_A(r) = \int_0^{2\pi} p_{A,\Theta}(r,\varphi)\,d\varphi = \frac{r}{\sigma^2}e^{-r^2/2\sigma^2} \qquad (r \geq 0),$$

Note that $p_A(r) = 0$ for $r < 0$, so that

$$p_A(r) = \frac{r}{\sigma^2}e^{-r^2/2\sigma^2}\,\mathbf{1}_{[0,\infty)}(r),$$

which is the Rayleigh density function. (Random variables having the Rayleigh distribution will be denoted as $\mathcal{R}(\sigma)$ random variables.) Since the brightness of a pixel in a B-scan image is proportional to the amplitude A, we may think of

$$P(A \leq s) = \int_0^s \frac{r}{\sigma^2}e^{-r^2/2\sigma^2}\,dr$$

as the probability that a given pixel will have brightness $\leq s$, for all $s \geq 0$.

It is well known and can easily be established that $p_A(r)$ has mean $\sigma\sqrt{\pi/2}$ and second moment $2\sigma^2$. Thus, variance is proportional to the square of the mean.

Remark 2.2. Let u denote the 'real' return signal amplitude, assuming the various phasors would all be deterministic and identical. The power of this signal would then be cu^2 for some constant c. Thus in the probabilistic model, the mean powers of the reflections from all small scatterers should combine to this value, that is,

$$cu^2 = \sum_{k=1}^N E\left[c\left(\frac{A_k}{\sqrt{N}}\right)^2\right].$$

Hence,

$$u^2 = \frac{1}{N}\sum_{k=1}^N E\left[A_k^2\right] = \frac{1}{N}\sum_{k=1}^N \rho = \rho,$$

so that

$$\sigma = \sqrt{\frac{\rho}{2}} = \frac{u}{\sqrt{2}}.$$

We emphasize that in this model, noise essentially arises from the fact that the signals returning from the various scatterers within a resolution cell have different phases.

Model II: One preferred reflection leading to the Rician distribution

This model mixes specular with nonspecular reflections. On assumes that within a resolution cell there is first of all one well defined main scatterer of specular type, but that there is also a large number of very small nonspecular scatterers which contribute to noise as in the previous model. The signal from the main scatterer is deterministic, and for simplicity we may assume that it has zero phase and amplitude a_o,

$$a_o\cos\omega t.$$

On the other hand, the signals from the remaining scatterers are probabilistic, following the assumptions of the previous model. Thus, the sum of all returning signals results in a random signal

$$A \cos\left(\omega t - \Theta\right) = a_o \cos\left(\omega t\right) + \frac{1}{\sqrt{N}} \sum_{k=1}^{N} A_k \cos\left(\omega t - \Theta_k\right),$$

or expressed by phasors,

$$A e^{j\Theta} = a_o + \frac{1}{\sqrt{N}} \sum_{k=1}^{N} A_k e^{j\Theta_k}.$$

The real and imaginary parts are

$$\mathfrak{r} := \mathfrak{Re}(A e^{j\Theta}) = a_o + \frac{1}{\sqrt{N}} \sum_{k=1}^{N} A_k \cos\Theta_k$$

$$\mathfrak{i} := \Im(A e^{j\Theta}) = \frac{1}{\sqrt{N}} \sum_{k=1}^{N} A_k \sin\Theta_k.$$

As $N \to \infty$, the two sums over k become again independent and normally distributed random variables, and because of the deterministic term a_o, $\mathfrak{r}$ becomes $\mathcal{N}(a_o, \sigma^2)$, while $\mathfrak{i}$ remains $\mathcal{N}(0, \sigma^2)$. That is, their probability density functions are

$$p_{\mathfrak{r}}(x) = \frac{1}{\sqrt{2\pi}\sigma} e^{-(x-a_o)^2/2\sigma^2} \qquad \text{and} \qquad p_{\mathfrak{i}}(y) = \frac{1}{\sqrt{2\pi}\sigma} e^{-y^2/2\sigma^2}.$$

Thus, the joint probability function becomes

$$p_{\mathfrak{r},\mathfrak{i}}(x,y) = p_{\mathfrak{r}}(x) p_{\mathfrak{i}}(y) = \frac{1}{2\pi\sigma^2} e^{-[(x-a_o)^2+y^2]/2\sigma^2}.$$

Changing to polar coordinates,

$$p_{A,\Theta}(r,\varphi) = \frac{r}{2\pi\sigma^2} e^{-(r^2+a_o^2)/2\sigma^2} e^{a_o r \cos\varphi/\sigma^2}.$$

Hence the amplitude A of the return signal has the probability density function

$$p_A(r) = \int_0^{2\pi} p_{A,\Theta}(r,\varphi)\, d\varphi = \frac{r}{2\pi\sigma^2} e^{-(r^2+a_o^2)/2\sigma^2} \int_0^{2\pi} e^{(a_o r/\sigma^2)\cos\varphi}\, d\varphi$$

for $r \geq 0$, while $p_A(r) = 0$ for $r < 0$. We here recall the modified Bessel functions of the first kind, of zero and first orders,

$$I_0(s) = \frac{1}{\pi} \int_0^{\pi} e^{s\cos\varphi}\, d\varphi \qquad \text{and} \qquad I_1(s) = \frac{1}{\pi} \int_0^{\pi} e^{s\cos\varphi} \cos\varphi\, d\varphi$$

Thus,

$$p_A(r) = \frac{r}{\sigma^2} e^{-(a_o^2+r^2)/2\sigma^2} I_0\left(\frac{a_o r}{\sigma^2}\right) \mathbf{1}_{[0,\infty)}(r).$$

This is called a *Rician* density function. Its mean is known to be

$$\sqrt{\frac{\pi}{2}}\sigma e^{-k}\left[(1+2k) I_0(k) + 2k I_1(k)\right]$$

where $k = a_o^2/4\sigma^2$, and its second moment is

$$2\sigma^2 + a_o^2.$$

2.3 Variational Noise Reduction Models

2.3.1 Calculus of Variations

Calculus of Variations is a field of mathematics that deals with functionals. Such functionals may be formed as integrals involving an unknown function together with some of its derivatives. The interest is then in finding extremal functions which make the functional attain a maximum or a minimum value. There are numerous monographs establishing the existence and characterization of extrema available in the literature. In many cases, extremal functions or curves can be expressed as solutions to differential equations, and we will only review the most classical of these results:

Theorem 1. *Let $\Omega \subset \mathbb{R}^n$ be a bounded, open set with Lipschitz boundary[1] $\partial\Omega$. Let $F = F(x, u, \xi) \in C^2(\overline{\Omega} \times \mathbb{R} \times \mathbb{R}^n)$ and consider the functional*

$$I(u) = \int_\Omega F\left(x, u(x), \nabla u(x)\right)\, dx, \qquad u \in C^1(\overline{\Omega}),\ u = u_o\ on\ \partial\Omega.$$

If $\hat{u} \in C^2(\overline{\Omega})$ is a minimizer of I, i.e. $I(\hat{u}) \le I(u)\ \forall u \in C^1(\overline{\Omega})$, then $\hat{u}$ satisfies the Euler Lagrange *equation*

$$\sum_{i=1}^{n} \frac{\partial}{\partial x_i} \left[F_{\xi_i}(x, u, \nabla u)\right] - F_u(x, u, \nabla u) = 0, \qquad x \in \overline{\Omega}. \tag{2.8}$$

Conversely, if $(u, \xi) \mapsto F(x, u, \xi)$ is convex for every $x \in \overline{\Omega}$, and if $\hat{u} \in C^2(\overline{\Omega})$ is a solution of (2.8), then it is a minimizer of I.

This theorem is available for larger classes of functions, for example for functions u in the Sobolev space $W^{1,p}(\Omega)$; however, minimizers $\hat{u}$ which are not twice differentiable will then be only weak solutions to the Euler-Lagrange equation, see Theorem 3.11 in [5].

2.3.2 Review of Existing Variational Models

Throughout, let Ω denote an open, bounded subset of the plane representing the image area. The function $u_o(x, y)$, $(x, y) \in \Omega$, will represent the original, noiseless image. The noise is represented by the function $n(x, y)$, the noisy image by $f(x, y)$, and the desired denoised image by $u(x, y)$. The Euclidean norm is denoted by $|\cdot|$.

One essentially distinguishes between two types of noise: Additive noise

$$f(x, y) = u_o(x, y) + n(x, y)$$

is used, for example, to model white noise. Multiplicative noise

$$f(x, y) = u_o(x, y)n(x, y)$$

is used when the image noise is proportional to the amplitude of the signal.

The following variational approaches for image noise reduction have appeared in the literature.

---

[1] The definition of Lipschitz boundary is given in Chapter 3.

1. **The ROF model**

   In 1992, Rudin, Osher, and Fatemi (ROF) [19] presented this mathematical denoising model which is based on the additive noise model, employing the functional

   $$F(u) = \beta \int_\Omega |\nabla u| + \int_\Omega (u - f)^2.$$

   Here, as throughout, all integrals are with regards to the Lebesgue measure. The functional F to be minimized thus consists of two components: The first component is to minimize the average gradient within the denoised image, while the second term is a data-fidelity term used to minimize the mean square difference between the noisy and the denoised image. The coefficient β assigns weights to each of the two components.

   By calculus of variations, the solution of this problem is obtained when its Euler-Lagrange differential equation is satisfied,

   $$\frac{\partial}{\partial x}\left(\frac{u_x}{\sqrt{u_x^2 + u_y^2}}\right) + \frac{\partial}{\partial y}\left(\frac{u_y}{\sqrt{u_x^2 + u_y^2}}\right) + \frac{2}{\beta}(f - u) = 0,$$

   where $\dfrac{\partial u}{\partial N} = 0$ on $\partial\Omega$ and N is the vector normal to the boundary $\partial\Omega$. This equation may be written in the form

   $$\text{div}\left(\frac{\nabla u}{|\nabla u|}\right) + \frac{2}{\beta}(f - u) = 0.$$

2. **A variational approach for Poisson noise – The Le Model**

   Le, Chatrand and Asaki [16] modified the ROF model to present a data-fidelity term which is suitable for Poisson noise. The model is to minimize the functional

   $$G(u) = \beta \int_\Omega |\nabla u| + \int_\Omega (u - f \ln u).$$

   The Euler-Lagrange differential equation for solving this problem is

   $$\text{div}\left(\frac{\nabla u}{|\nabla u|}\right) + \frac{1}{\beta u}(f - u) = 0,$$

   where $\dfrac{\partial u}{\partial N} = 0$ on $\partial\Omega$.

3. **A variational approach to remove multiplicative SAR speckle noise – The AA model**

   Aubert and Aujol [1] focus on the problem of multiplicative noise removal for SAR radar images. The noise is modeled by an exponential distribution, which results in the functional

   $$H(u) = \beta \int_\Omega |\nabla u| + \int_\Omega \left(\ln u + \frac{f}{u}\right)$$

to be minimized by solving the Euler-Lagrange differential equation

$$\text{div}\left(\frac{\nabla u}{|\nabla u|}\right) + \frac{1}{\beta u^2}(f - u) = 0$$

where $\frac{\partial u}{\partial N} = 0$ on $\partial\Omega$.

2.3.3   The Proposed Model

We are now ready to present our proposed model for the removal of ultrasound speckle noise. We will employ Model I of speckle noise: the brightness or intensity of a pixel in the noisy ultrasound image is a Rayleigh random variable and thus has density function

$$p_\sigma(r) = \frac{r}{\sigma^2} e^{-\frac{r^2}{2\sigma^2}} \qquad (r \geq 0), \tag{2.9}$$

where σ is a parameter which may vary from pixel to pixel. The variance of p_σ is a measure of noise, and since the variance is proportional to the square of the mean, noise in this model may be considered to be of multiplicative type.

The model for noise removal is being developed in a way which is similar to the AA model [1]. The difference is that the AA model assumes that the signal receiver measures the energy of the signal, which results in the noisy pixel intensity to possess an exponential distribution. In our model on the other hand, as we are dealing with ultrasound images, the receiver of the ultrasound signal measures the signal's amplitude, which results in the noisy pixel intensity to possess a Rayleigh distribution.

To begin with, we assume that the image takes the form of a square of size $(N - 1) \times (N - 1)$. This is not really a restriction, as any image of square shape can be scaled to this size. The values $u_o(x, y)$, $f(x, y)$ and $u(x, y)$ represent the intensities of the unknown noiseless image, the given noisy image and the desired denoised image, respectively, at location (x, y), and may also be denoted by subscripts, for example $f_{x,y}$ instead of $f(x, y)$. Thus, these functions all take on positive values only on Ω. The noiseless image is unknown, the noisy image is being measured, while the denoised image u to be found should be a good approximation to u_o.

Throughout, we will switch freely between this continuous and a discrete model: In the discrete model, the image is pixellated as

$$\Omega = \{(x, y) \ : \ x, y = 0, \ldots, N - 1\},$$

so that $u_o(x, y)$, $f(x, y)$ and $u(x, y)$ represent the image intensities at pixel (x, y). For a large number of pixels of small size, after rescaling Ω to its original size, the discrete model can be considered a good approximation to the continuous model.

We let $\mathcal{X}$ denote the space of all possible images. Thus, elements of $\mathcal{X}$ are functions $u : \Omega \to (0, \infty)$. This is a probability space with unknown probability measure. From the probabilistic point

of view, the noiseless image and the noisy image are random variables U and F on X, respectively, and we are going to find an image u to which U is the most likely, given the observed noisy image f. That is, we must find u which maximizes

$$P(U = u | F = f).$$

This image u will then be considered as the denoised image. The distributions of U and F will be discussed below. It turns out that the distribution of F is known at the pixel level only, thus we now proceed to consider each pixel individually.

Given any random variable V on $\mathcal{X}$, $V_{x,y}$ will denote the corresponding random variable of pixel intensity at pixel (x, y). Note that $V_{x,y}$ is a random variable on $\mathbb{R}$. Here we make an important assumption: We assume that the image intensities $U_{x,y}$ (and similarly the image intensities $F_{x,y}$) at different pixels are independent. Thus,

$$P(U = u | F = f) = \prod_{(x,y) \in \Omega} P(U_{x,y} = u_{x,y} | F_{x,y} = f_{x,y}),$$

where $u_{x,y} = u(x, y)$ and $f_{x,y} = f(x, y)$. *Bayes' Rule* says that

$$P(U_{x,y} = u_{x,y} | F_{x,y} = f_{x,y}) = \frac{P(F_{x,y} = f_{x,y} | U_{x,y} = u_{x,y}) \, P(U_{x,y} = u_{x,y})}{P(F_{x,y} = f_{x,y})},$$

hence we need to maximize

$$\frac{\prod_{(x,y) \in \Omega} P(F_{x,y} = f_{x,y} | U_{x,y} = u_{x,y}) \, P(U_{x,y} = u_{x,y})}{\prod_{(x,y) \in \Omega} P(F_{x,y} = f_{x,y})}.$$

Since the denominator does not depend on u, it suffices to maximize

$$\prod_{(x,y) \in \Omega} P(F_{x,y} = f_{x,y} | U_{x,y} = u_{x,y}) \, P(U_{x,y} = u_{x,y}). \tag{2.10}$$

Now by assumption, each $F_{x,y}$ is a Rayleigh random variable with probability density

$$P(F_{x,y} = f_{x,y}) = p_\sigma(f_{x,y}) = \frac{f_{x,y}}{\sigma^2} e^{-\frac{[f_{x,y}]^2}{2\sigma^2}}$$

where as outlined in Remark 2.2, $\sigma = \sigma(x, y) = u(x, y)/\sqrt{2} = u_{x,y}/\sqrt{2}$. Then

$$P(F_{x,y} = f_{x,y} | U_{x,y} = u_{x,y}) = p_\sigma(f_{x,y}) = \frac{2 f_{x,y}}{[u_{x,y}]^2} e^{-\left[\frac{f_{x,y}}{u_{x,y}}\right]^2}.$$

Expression (2.10) becomes

$$\left(\prod_{(x,y) \in \Omega} \frac{2 f_{x,y}}{[u_{x,y}]^2} e^{-\left[\frac{f_{x,y}}{u_{x,y}}\right]^2} \right) \left(\prod_{(x,y) \in \Omega} P(U_{x,y} = u_{x,y}) \right)$$

that is,

$$\left(\prod_{(x,y) \in \Omega} \frac{2 f_{x,y}}{[u_{x,y}]^2} e^{-\left[\frac{f_{x,y}}{u_{x,y}}\right]^2} \right) P(U = u). \tag{2.11}$$

Since the function $\ln(x)$ is increasing, maximizing (2.11) is equivalent to minimizing

$$-\ln\big[P(U=u)\big] + \sum_{(x,y)\in\Omega}\left(\left[\frac{f_{x,y}}{u_{x,y}}\right]^2 + 2\ln u_{x,y} - \ln f_{x,y} - \ln 2\right).$$

We regard this as a discrete approximation of the functional

$$E(u) = -\ln\Phi(u) + \int_\Omega\left(\frac{f^2}{u^2} + 2\ln u - \ln f - \ln 2\right),$$

where $\Phi(u)$ is the density function of the random variable U.

Now Green [10] has shown that for the model of a variational approach, this density function is

$$\Phi(u) = e^{-\beta\int_\Omega|\nabla u|}$$

where β is a positive parameter. Hence, functional $E(u)$ becomes

$$E(u) = \beta\int_\Omega|\nabla u| + \int_\Omega\left(\frac{f^2}{u^2} + 2\ln u - \ln f - \ln 2\right).$$

Since the last two terms independent of u, it suffices to minimize the functional

$$E(u) = \int_\Omega|\nabla u| + \frac{1}{\beta}\int_\Omega\left(2\ln u + \frac{f^2}{u^2}\right). \tag{2.12}$$

The formal Euler-Lagrange equation for minimizing $E(u)$ is then

$$\operatorname{div}\left(\frac{\nabla u}{|\nabla u|}\right) + \frac{2}{\beta u^3}\left(f^2 - u^2\right) = 0. \tag{2.13}$$

Note that Theorem 1 does not apply here. In fact, in the notation of that theorem,

$$F(x,u,\xi) = |\xi| + \frac{1}{\beta}\left(2\ln u + \frac{f(x)^2}{u^2}\right),$$

which is defined for $u > 0$ only. If we change variables, $u = e^z$ in (2.12), then we obtain

$$F(x,z,\xi) = e^z|\xi| + \frac{1}{\beta}\left(2z + f(x)^2 e^{-2z}\right),$$

which is defined for all $z \in \mathbb{R}$. However, both functions F are still not differentiable at $\xi = 0$, and the validity of the Euler-Lagrange equation must be justified differently. This problem is discussed in the next chapter.

Chapter 3

Mathematical Treatment of the Model

Consider the problem of existence and uniqueness of solutions of our model: find a minimizer of the functional (2.12),

$$E(u) = \underbrace{\int_\Omega |\nabla u|}_{\phi(u)} + \lambda \underbrace{\int_\Omega \left[2 \ln u + \frac{f^2}{u^2} \right]}_{J(u)} \tag{3.1}$$

where we have set $\lambda = \beta^{-1}$. We will shortly see that the set $BV(\Omega)$ of functions of bounded variation is the largest class of functions for which the functional ϕ can be defined, and simple compactness arguments are available for this class which yield the existence of minimizers. Uniqueness of minimizers will only be obtained after mildly restricting the class of functions u allowed, to guarantee that the functional J is convex. Our exposition parallels that of [1], but with a different data-fidelity term $J(u)$. First we review the concepts and properties to be used, most of which are assembled from [7].

3.1 Preliminaries

Throughout, Ω will denote an open and bounded subset of $\mathbb{R}^n$. Unless specified otherwise, integrals will be with respect to the Lebesgue measure μ on $\mathbb{R}^n$.

1. Let $C^1_c(\Omega, \mathbb{R}^n)$ denote the set of continuously differentiable vector valued functions which are defined on Ω and have compact support. This is a normed linear space in the norm

$$\|\varphi\|_\infty = \max_{\omega \in \Omega} |\varphi(\omega)|$$

where $|x|$ denotes the Euclidean norm in $\mathbb{R}^n$, $|x| = (x_1^2 + \ldots x_n^2)^{1/2}$ for $x = (x_1, \ldots, x_n)$.

2. A function $u \in L^1(\Omega)$ is said to be of *bounded variation* in Ω, if

$$\|Du\|(\Omega) = \sup \left\{ \int_\Omega u \operatorname{div} \varphi \ : \ \varphi \in C^1_c(\Omega, \mathbb{R}^n), \ \|\varphi\|_\infty \leq 1 \right\} < \infty.$$

$\|Du\|(\Omega)$ is called the *total variation of u on* Ω. We set

$$BV(\Omega) = \{u \in L^1(\Omega) : \|Du\|(\Omega) < \infty\}.$$

Clearly, $BV(\Omega)$ is a linear subspace of $L^1(\Omega)$, and $\|Du\|(\Omega)$ is a seminorm on $BV(\Omega)$. Consequently,

$$\|u\|_{BV(\Omega)} := \|Du\|(\Omega) + \|u\|_{L^1(\Omega)}$$

is a norm, and it turns out that $BV(\Omega)$ is a Banach space in this latter norm.

3. Let $u \in L^1(\Omega) \cap C^1(\Omega)$. Since the functions $\varphi \in C_c^1(\Omega, \mathbb{R}^n)$ are compactly supported, one may integrate by parts to obtain

$$\int_\Omega u \operatorname{div}\varphi = - \int_\Omega \varphi \cdot \nabla u \leq \left| \int_\Omega \varphi \cdot \nabla u \right| \leq \int_\Omega |\varphi \cdot \nabla u| \leq \int_\Omega |\varphi| \, |\nabla u| < \infty,$$

which shows that $u \in BV(\Omega)$ and $\|Du\|(\Omega) \leq \int_\Omega |\nabla u|$.

Conversely, set

$$g(\omega) = \begin{cases} \dfrac{\nabla u(\omega)}{|\nabla u(\omega)|} & \text{if } \nabla u(\omega) \neq 0 \\[2mm] 0 & \text{if } \nabla u(\omega) = 0. \end{cases}$$

By density of $C_c^1(\Omega, \mathbb{R})$ in $L^2(\Omega)$, there exists a sequence $\{\varphi_k\}$ in $C_c^1(\Omega, \mathbb{R}^n)$ with $|\varphi_k| \leq 1$ converging to g in the norm of $L^2(\Omega, \mathbb{R}^n)$. Hence

$$\int_\Omega |\nabla u| = \int_\Omega g \cdot \nabla u = \int_\Omega (\lim_{k\to\infty} \varphi_k) \cdot \nabla u = \lim_{k\to\infty} \int_\Omega \varphi_k \cdot \nabla u = -\lim_{k\to\infty} \int_\Omega (-\varphi_k) \cdot \nabla u$$

$$\leq \sup \left\{ -\int_\Omega \varphi \cdot u \; : \; \varphi \in C_c^1(\Omega, \mathbb{R}^n), \; \|\varphi\|_\infty \leq 1 \right\} = \|Du\|(\Omega).$$

We thus have shown that $L^1(\Omega) \cap C^1(\Omega) \subset BV(\Omega) \subset L^1(\Omega)$, and that

$$\int_\Omega |\nabla u| = \|Du\|(\Omega) \qquad \forall \, u \in L^1(\Omega) \cap C^1(\Omega).$$

This allows us to extend the functional ϕ in (3.1) to all of $BV(\Omega)$ by setting

$$\phi(u) = \|Du\|(\Omega) \qquad \forall u \in BV(\Omega). \tag{3.2}$$

4. Some properties of functions of bounded variation:

Theorem 2. (see [7]). *Let $u \in BV(\Omega)$. Then there exist a finite Radon measure ν on Ω and a measurable function $\sigma : \Omega \to \mathbb{R}^n$ satisfying*

(a) $|\sigma(\omega)| = 1$ a.e. $\omega \in \Omega$,

(b) $\displaystyle \int_\Omega u \operatorname{div}\varphi = - \int_\Omega \varphi \cdot \sigma \, d\nu$ for all $\varphi \in C_c^1(\Omega, \mathbb{R}^n)$.

Theorem 3. (see [7]). *Let $\{u_k\} \subset BV(\Omega)$ and suppose that $u_k \to u$ in the norm of $L^1(\Omega)$. Then*

$$\|Du\|(\Omega) \leq \liminf_k \|Du_k\|(\Omega).$$

5. The next theorem requires that the boundary $\partial\Omega$ of Ω be sufficiently regular. A frequently used condition is that $\partial\Omega$ be Lipschitz. Loosely speaking, this means that locally, $\partial\Omega$ is the graph of a Lipschitz continuous function.

To be precise, we say that Ω has *Lipschitz boundary*, if for every $\omega \in \partial\Omega$ there exist $\epsilon > 0$ and a Lipschitz function $H : \mathbb{R}^{n-1} \to \mathbb{R}$ so that – after rotating and relabeling the coordinate axes if necessary –

$$\Omega \cap Q(\omega, \epsilon) = \{\, y \in \mathbb{R}^n : H(y_1, \ldots, y_{n-1}) < y_n \,\} \cap Q(\omega, \epsilon)$$

where $Q(\omega, \epsilon)$ is the open n-cube $\{y \in \mathbb{R}^n : |y_j - \omega_j| < \epsilon, \ j = 1, \ldots, n\}$. Recall here that H is Lipschitz if there exists a constant $K > 0$ so that

$$|H(x) - H(y)| \leq K|x - y| \qquad \forall x, y \in \mathbb{R}^{n-1}.$$

The next theorem says that subsets of $BV(\Omega)$ which take the form of closed, bounded balls under $\|\cdot\|_{BV(\Omega)}$ are even compact in the L^1-norm. It will be used to prove the existence of minimizers.

Theorem 4. *Let Ω be an open bounded subset of $\mathbb{R}^n$ with Lipschitz boundary. Let $\{u_k\}$ be a sequence in $BV(\Omega)$ satisfying*

$$\|u_k\|_{BV(\Omega)} \leq M, \qquad \forall k.$$

Then there exist a subsequence $\{u_{k_j}\}$ and a function $u \in BV(\Omega)$ such that

$$u_{k_j} \to u$$

in the norm of $L^1(\Omega)$.

6. Convexity arguments will be employed for proving the uniqueness of minimizers.

Recall that a subset S of a vector space X is said to be *convex* if $y, z \in S$ implies that the line segment

$$L = \{\, \alpha y + (1 - \alpha)z \ : \ 0 \leq \alpha \leq 1 \,\}$$

is a subset of S.

Next let S be a convex set. A real functional E on S is said to be *convex* if for every $y, z \in S$,

$$E\big(\alpha y + (1 - \alpha)z\big) \leq \alpha E(y) + (1 - \alpha)E(z),$$

where $0 \leq \alpha \leq 1$. In addition, if for every $y, z \in S$, $y \neq z$,

$$E\big(\alpha y + (1-\alpha)z\big) < \alpha E(y) + (1-\alpha)E(z),$$

where $0 < \alpha < 1$, then E is said to be a *strictly convex*.

Theorem 5. *Let E be a real valued functional on a set S. Let $Q \subseteq S$ be convex, and suppose, there exists a minimizer $\hat{u} \in Q$ of E, that is,*

$$E(\hat{u}) \leq E(u) \qquad \forall\, u \in S.$$

If E is strictly convex, then $\hat{u}$ is the unique minimizer of E in Q.

Proof. Suppose to the contrary that there exists another minimizer $\tilde{u}$ of E in Q, that is, $\tilde{u} \in Q$, $\tilde{u} \neq \hat{u}$, and

$$E(\tilde{u}) \leq E(u) \qquad \forall\, u \in S.$$

Then in particular,

$$E(\tilde{u}) = E(\hat{u}) =: b.$$

Set

$$v = \frac{1}{2}\hat{u} + \frac{1}{2}\tilde{u} \in Q.$$

As $\hat{u} \neq \tilde{u}$, we have by strict convexity of E on Q that

$$E(v) < \frac{1}{2}E(\hat{u}) + \frac{1}{2}E(\tilde{u}) = b$$

contradicting the fact that $\hat{u}$ minimizes E. $\qquad\square$

Proposition 6. *If $F : (a,b) \to \mathbb{R}$ is continuously twice differentiable and $F''(u) > 0$, for every $u \in (a,b)$ then, F is strictly convex.*

Proof. This is a standard result from calculus, see [20] for example. $\qquad\square$

3.2 Existence and Uniqueness of Minimizers

From here on, we will employ the following assumptions:

(A1) Ω is a bounded, open subset of $\mathbb{R}^2$ with Lipschitz boundary,

(A2) $S(\Omega) = \{u \in BV(\Omega) : u > 0 \text{ a.e.}\}$. The denoised image u is an element of $S(\Omega)$.

(A3) The noisy image f is an element of $L^\infty(\Omega)$ and is essentially bounded below away from zero, i.e. there exist real numbers m and M so that $0 < m \leq f(\omega) \leq M$ a.e.

Furthermore, μ will denote the Lebesgue measure on $\mathbb{R}^2$.

Motivated by (3.1) and (3.2), we want to find minimizers $u \in BV(\Omega)$ for the functional

$$E(u) = \phi(u) + J(u) = \|Du\|(\Omega) + \lambda \int_\Omega \left[2\ln u + \frac{f^2}{u^2} \right]. \tag{3.3}$$

It is not clear from the outset that $J(u)$ should be defined for all $u \in S(\Omega)$. Let us verify that this is indeed true. Given $\gamma > 0$, consider the function

$$h(x) = 2\ln x + \frac{\gamma^2}{x^2} \qquad (x > 0). \tag{3.4}$$

Its derivative is

$$h'(x) = \frac{2}{x} \left[1 - \frac{\gamma^2}{x^2} \right].$$

Thus, $h(x)$ is strictly decreasing on $(0, \gamma)$ and strictly increasing on (γ, ∞), and takes the absolute minimum value at $x = \gamma$,

$$h(\gamma) = 2\ln\gamma + 1 \le h(x) = 2\ln x + \frac{\gamma^2}{x^2} \qquad \forall x > 0.$$

Thus if $u \in S(\Omega)$, then for every $\omega \in \Omega$,

$$2\ln f(\omega) + 1 \le 2\ln u(\omega) + \frac{f(\omega)^2}{u(\omega)^2}.$$

Since f is essentially bounded below, this implies that $J(u)$ is defined (it may take the value ∞), and

$$J(u) \ge (2\ln m + 1)\mu(\Omega) \qquad \forall u \in S(\Omega). \tag{3.5}$$

Since $\phi(u) \ge 0$, it follows that

$$b := \inf\{\, E(u) : u \in S(\Omega) \,\} \ge (2\ln m + 1)\mu(\Omega). \tag{3.6}$$

We first prove the existence of minimizers.

Theorem 7. *Let Ω and f satisfy (A1) and (A3), respectively. Then there exists $\hat{u} \in S(\Omega)$ satisfying*

1. *$m \le \hat{u}(\omega) \le M$ a.e.*

2. *$E(\hat{u}) \le E(u)$ for all $u \in S(\Omega)$.*

Proof. Let $\{u_n\}$ be any minimizing sequence in $S(\Omega)$, that is,

$$\lim_{n\to\infty} E(u_n) = b,$$

where b is as in (3.6). We begin by modifying this sequence so that $m \le u_n(\omega) \le M$.

Since the function $h(x)$ in (3.4) is increasing on $[\gamma, \infty)$, it follows that for all $M_o \ge \gamma$,

$$2\ln[\min(x, M_o)] + \frac{\gamma^2}{\min(x, M_o)^2} \le 2\ln x + \frac{\gamma^2}{x^2}, \qquad x > 0.$$

Thus for any $u \in S(\Omega)$,

$$2 \ln \left[\min(u(\omega), M)\right] + \frac{f(\omega)^2}{\min(u(\omega), M)^2} \leq 2 \ln u(\omega) + \frac{f(\omega)^2}{u(\omega)^2} \qquad \forall \omega \in \Omega$$

which implies that

$$J\left(\min(u, M)\right) \leq J(u).$$

Now it is known that $\min(u, M) \in BV(\Omega)$ and

$$\phi\left(\min(u, M)\right) \leq \phi(u),$$

(see for example the proof of Lemma 1 in [13]), and hence $E\left(\min(u, M)\right) \leq E(u)$. It follows that we may replace each u_n with $\min(u_n, M)$; the sequence $\{u_n\}$ will remain minimizing.

In a similar way, since the function $h(x)$ in (3.4) is decreasing on $(0, \gamma]$, it follows that for all $M_o \leq \gamma$,

$$2 \ln \left[\max(x, M_o)\right] + \frac{\gamma^2}{\max(x, M_o)^2} \leq 2 \ln x + \frac{\gamma^2}{x^2}, \qquad x > 0.$$

Thus for any $u \in S(\Omega)$,

$$2 \ln \left[\max(u(\omega), m)\right] + \frac{f(\omega)^2}{\max(u(\omega), m)^2} \leq 2 \ln u(\omega) + \frac{f(\omega)^2}{u(\omega)^2} \qquad \forall \omega \in \Omega$$

which implies that

$$J\left(\max(u, m)\right) \leq J(u).$$

Since (again using the arguments in the proof of Lemma 1 of [13]) $\max(u, m) \in BV(\Omega)$ and

$$\phi\left(\max(u, m)\right) \leq \phi(u),$$

then $E\left(\max(u, m)\right) \leq E(u)$. It follows that we may replace each u_n with $\max(u_n, m)$; the sequence $\{u_n\}$ will remain minimizing. We thus have shown that we may assume that

$$m \leq u_n(\omega) \leq M \tag{3.7}$$

for all $\omega \in \Omega$.

We next employ this sequence to prove the existence of the minimizer $\hat{u}$. The argument is standard. As $\{u_n\}$ minimizes E, the sequence $\{E(u_n)\}$ is bounded, hence the sequence $\{\|Du_n\|(\Omega)\}$ is bounded. Furthermore, by (3.7), the sequence $\{u_n\}$ is bounded in the norm of $L^1(\Omega)$. Hence, $\{u_n\}$ is a bounded sequence in the norm of $BV(\Omega)$. Thus by Theorem 4, after having replaced u_n with a suitable subsequence, there exists $\hat{u} \in BV(\Omega)$ such that $u_n \to \hat{u}$ in the norm $\|\cdot\|_{L^1(\Omega)}$. Since every convergent sequence in $L^1(\Omega)$ possesses a subsequence $\{u_{n_k}\}$ converging pointwise a.e. to the same limit, then assertion 1. follows.

Now by Theorem 3,

$$\|D\hat{u}\|(\Omega) \leq \liminf_{k} \|Du_{n_k}\|(\Omega). \tag{3.8}$$

On the other hand, by (3.7) we can apply the Dominated Convergence Theorem to obtain

$$
\begin{aligned}
J(\hat{u}) &= \int_{\Omega} \lim_{k \to \infty} \left(2 \ln u_{n_k} + \frac{f^2}{u_{n_k}^2} \right) d\mu \\
&= \lim_{k \to \infty} \int_{\Omega} \left(2 \ln u_{n_k} + \frac{f^2}{u_{n_k}^2} \right) d\mu = \lim_{k \to \infty} J(u_{n_k}).
\end{aligned}
\tag{3.9}
$$

Combining expressions (3.8) and (3.9) then

$$
\begin{aligned}
E(\hat{u}) &= \|D\hat{u}\|(\Omega) + J(\hat{u}) \\
&\leq \liminf_{k} \|Du_{n_k}\|(\Omega) + \lim_{k \to \infty} J(u_{n_k}) \\
&\leq \liminf_{k} \left[\|Du_{n_k}\|(\Omega) + J(u_{n_k}) \right] \\
&= \liminf_{k} E(u_{n_k}) = b
\end{aligned}
$$

since the sequence $\{u_n\}$ minimizes E. This proves the existence of a minimizer $\hat{u}$. $\qquad\square$

There is only a partial result on the uniqueness of the minimizer. The reason is that J is strictly convex only on $Q(\Omega) = \{ u \in S(\Omega) : u(w) \leq \sqrt{3}f(\omega) \text{ a.e.} \}$. In fact, as

$$
h''(x) = \frac{2}{x^2} \left[\frac{3\gamma^2}{x^2} - 1 \right]
$$

then h is strictly convex if and only if $0 < x < \sqrt{3}\gamma$. It follows that whenever $0 < u_1, u_2 < \sqrt{3}f$ a.e., then for all $0 < \lambda < 1$,

$$
F\big(\lambda u_1 + (1 - \lambda)u_2\big) < \lambda F(u_1) + (1 - \lambda)F(u_2) \qquad \text{a.e.}
$$

where $F(u) = 2\ln(u) + \frac{f^2}{u^2}$, and hence

$$
J\big(\lambda u_1 + (1 - \lambda)u_2\big) < \lambda J(u_1) + (1 - \lambda)J(u_2).
$$

We also observe that $Q(\Omega)$ is convex and non-empty, as f is essentially bounded below by $m > 0$. We thus have the following existence and uniqueness result.

Theorem 8. *Let Ω and f satisfy (A1) and (A3), respectively. Then there exists at most one $\hat{u} \in Q(\Omega)$ satisfying*

$$
E(\hat{u}) \leq E(u) \qquad \text{for all } u \in S(\Omega).
$$

Proof. By convexity of the norm $\|Du\|(\Omega)$ and strict convexity of J on $Q(\Omega)$, it follows that E is strictly convex on $Q(\Omega)$. Thus, Theorem 5 guarantees uniqueness of the minimizer $\hat{u} \in Q(\Omega)$ of E. $\qquad\square$

We note that the proof of Theorem 7 shows that $m \leq \hat{u}(\omega) \leq M$ a.e.

Corollary 9. *Let Ω and f satisfy (A1) and (A3), respectively. Then there exists a unique $\hat{u} \in Q(\Omega)$ satisfying*

$$E(\hat{u}) \leq E(u) \qquad \text{for all } u \in Q(\Omega).$$

Furthermore, $m \leq \hat{u}(\omega) \leq M$ a.e.

Proof. Existence of $\hat{u}$ can be derived from the proof of Theorem 7, now choosing $\{u_n\}$ to be a minimizing sequence in $Q(\Omega)$. Uniqueness of $\hat{u}$ follows from Theorem 5. $\square$

While uniqueness of minimizers $\hat{u} \in S(\Omega)$ cannot be proved in general, there is a monotonicity result, which is the analogue of Proposition 4.3 in [1] adapted to our choice of the functional J.

Theorem 10. *Let f_1 and f_2 satisfy condition (A3) with $f_1 \leq f_2$, and let u_1 and u_2 denote minimizers of E on $S(\Omega)$, corresponding to $f = f_1$ and $f = f_2$, respectively. Set*

$$A = \big\{\, w \in \Omega : f_1(\omega) < f_2(\omega) \,\big\}.$$

Then $u_1(\omega) \leq u_2(\omega)$ a.e. $\omega \in A$. In particular, if $f_1 < f_2$ a.e., then $u_1 \leq u_2$ a.e.

Proof. Set $u_1 \wedge u_2 = \min(u_1, u_2) \in S(\Omega)$ and $u_1 \vee u_2 = \max(u_1, u_2) \in S(\Omega)$. Since u_i is a minimizer of E for f_i $(i = 1, 2)$ we obtain

$$\phi(u_1 \wedge u_2) + \int_\Omega \left(2 \ln (u_1 \wedge u_2) + \frac{f_1^2}{(u_1 \wedge u_2)^2} \right) d\mu \geq \phi(u_1) + \int_\Omega \left(2 \ln u_1 + \frac{f_1^2}{u_1^2} \right) d\mu \qquad (3.10)$$

and

$$\phi(u_1 \vee u_2) + \int_\Omega \left(2 \ln (u_1 \vee u_2) + \frac{f_1^2}{(u_1 \vee u_2)^2} \right) d\mu \geq \phi(u_2) + \int_\Omega \left(2 \ln u_2 + \frac{f_2^2}{u_2^2} \right) d\mu. \qquad (3.11)$$

Adding both inequalities and employing the fact that $\phi(u_1 \wedge u_2) + \phi(u_1 \vee u_2) \leq \phi(u_1) + \phi(u_2)$ (see [4]), we obtain that

$$\int_\Omega \left(2 \ln (u_1 \wedge u_2) + \frac{f_1^2}{(u_1 \wedge u_2)^2} - 2 \ln u_1 - \frac{f_1^2}{u_1^2} \right.$$
$$\left. + 2 \ln (u_1 \vee u_2) + \frac{f_2^2}{(u_1 \vee u_2)^2} - 2 \ln u_2 - \frac{f_2^2}{u_2^2} \right) d\mu \geq 0. \qquad (3.12)$$

Note that the above integral, when integrated over the set $B = \{\, w \in \Omega : u_1(\omega) \leq u_2(\omega) \,\}$ only, equals zero. Thus, the integral over B^c is also non-negative. Now the integrand simplifies substantially when integrating over B^c, and we obtain

$$\int_{B^c} \left(\frac{f_1^2}{u_2^2} - \frac{f_1^2}{u_1^2} + \frac{f_2^2}{u_1^2} - \frac{f_2^2}{u_2^2} \right) d\mu \geq 0,$$

or equivalently,

$$\int_{B^c} \left(f_1^2 - f_2^2 \right) \left(\frac{1}{u_2^2} - \frac{1}{u_1^2} \right) d\mu \geq 0.$$

Since

$$\int_{A^c \cap B^c} \left(f_1^2 - f_2^2\right) \left(\frac{1}{u_2^2} - \frac{1}{u_1^2}\right) d\mu = \int_{A^c \cap B^c} 0 \, d\mu = 0$$

this implies that

$$\int_{A \cap B^c} \left(f_1^2 - f_2^2\right) \left(\frac{1}{u_2^2} - \frac{1}{u_1^2}\right) d\mu \geq 0.$$

Now as $\frac{1}{u_2^2} - \frac{1}{u_1^2} > 0$ on B^c while $f_1^2 - f_2^2 < 0$ on A, this implies that $A \cap B^c$ is a null set, and proves the theorem. $\qquad\square$

Chapter 4

Numerical Treatment of the Model

4.1 Numerical Scheme

We consider the solution of the Euler-Lagrange equation (2.13) as the steady state solution of the parabolic partial differential equation

$$u_t = \frac{\partial}{\partial x}\left(\frac{u_x}{\sqrt{u_x^2 + u_y^2}}\right) + \frac{\partial}{\partial y}\left(\frac{u_y}{\sqrt{u_x^2 + u_y^2}}\right) + \frac{2}{\beta u^3}(f^2 - u^2), \tag{4.1}$$

with initial condition $u(x, y, 0) = f(x, y)$ on Ω and the boundary condition $u(x, y, t) = f(x, y)$ on the boundary $\partial\Omega$ of the square Ω. In order to solve problem (4.1) numerically, the images are again pixellated, so that the spatial domain space is considered as an $N \times N$ square grid. The grid point (i, j) corresponds to location (x_i, y_j), $i = 0 \ldots N - 1, j = 0 \ldots N - 1$, where $x_i = ih$, $y_j = jh$ and $Nh = 1$.

Denote $u_{ij}^n = u(x_i, y_j, t_n)$ where $t_n = n\Delta t$, $n = 0, 1, 2, \ldots$ and Δt is step size, and set $u_{ij}^0 = f_{ij}$, Following [19], the numerical scheme of problem (4.1) is

$$
\begin{aligned}
u_{ij}^{n+1} &= u_{ij}^n \frac{\Delta t}{h}\left[\Delta_-^x\left(\frac{\Delta_+^x u_{ij}^n}{\sqrt{(\Delta_+^x u_{ij}^n)^2 + (m(\Delta_+^y u_{ij}^n, \Delta_-^y u_{ij}^n))^2}}\right)\right] \\
&\quad + \frac{\Delta t}{h}\left[\Delta_-^y\left(\frac{\Delta_+^y u_{ij}^n}{\sqrt{(\Delta_+^y u_{ij}^n)^2 + (m(\Delta_+^x u_{ij}^n, \Delta_-^x u_{ij}^n))^2}}\right)\right] \\
&\quad + \Delta t\left[\frac{2}{\beta(u_{ij}^n)^3}\left((f_{ij})^2 - (u_{ij}^n)^2\right)\right], \tag{4.2}
\end{aligned}
$$

with boundary conditions

$$
\begin{aligned}
u_{0j}^n &= f_{0j} \\
u_{(N-1)j}^n &= f_{(N-1)j} \\
u_{i0}^n &= f_{i0} \\
u_{i(N-1)}^n &= f_{i(N-1)}
\end{aligned}
$$

where $\Delta_\pm^x \Theta_{ij} = \pm(\Theta_{(i\pm1)j} - \Theta_{ij})$ and similarly for $\Delta_\pm^y \Theta_{ij}$. The step size Δt and h are chosen for stability such that

$$
\frac{\Delta t}{h} \leq 1.
$$

Here,

$$
m(a,b) = \frac{\mathrm{sgn}(a) + \mathrm{sgn}(b)}{2} \min(|a|, |b|).
$$

Note that if u_{ij}^n converges as $n \to \infty$, then $\dfrac{u_{ij}^{n+1} - u_{ij}^n}{\Delta t} \to 0$ as $n \to \infty$. Thus, the numerical solution of problem (4.2) will converge to an approximate solution of the equation

$$
\frac{\partial}{\partial x}\left(\frac{u_x}{\sqrt{u_x^2 + u_y^2}}\right) + \frac{\partial}{\partial y}\left(\frac{u_y}{\sqrt{u_x^2 + u_y^2}}\right) + \frac{2}{\beta u^3}(f^2 - u^2) = 0,
$$

where $u = f$ on $\partial\Omega$, which is the denoised image of our model.

4.2   Numerical Results

To verify the validity of our model, numerical experiments with sample images perturbed by noise were performed. The correlation coefficients between the original and the noisy images were compared with the correlation coefficients between the original and the reconstructed images. All experiments were done with MATLAB software version 7.2.

First, speckle noise with 0.02 variance was added to an original pattern image. The denoising algorithms used are the ROF model, the Le model, the AA model, and our proposed model. The correlation coefficient between the original image and the noisy image was 0.9678 while the correlation coefficients between the original image and the reconstructed images increased with an increasing number of iterative loops as shown in Table 4.1, and were higher than 0.9678 throughout.

Next, the Lenna image which is a well-known image in the field of image processing was used in our experiments. Speckle noise with 0.02 variance was added to the original image. Similarly, correlation coefficients were compared and they are shown in Table 4.2. The correlation coefficient between the original image and the noisy image is 0.9444, while the correlation coefficients between the original image and reconstructed images are all higher.

# of iterative loops	ROF Model	Le Model	AA Model	Proposed Model
0	0.9678	0.9678	0.9678	0.9678
200	0.9882	0.9960	0.9963	0.9963
250	0.9889	0.9971	0.9974	0.9974
300	0.9893	0.9978	0.9980	0.9980
350	0.9895	0.9981	0.9982	0.9982

Table 4.1: Correlation coefficients of reconstructed pattern images.

# of iterative loops	ROF Model	Le Model	AA Model	Proposed Model
0	0.9444	0.9444	0.9444	0.9444
80	0.9663	0.9725	0.9730	0.9730
120	0.9704	0.9798	0.9804	0.9804
160	0.9728	0.9843	0.9848	0.9848
200	0.9743	0.9868	0.9870	0.9871

Table 4.2: Correlation coefficients of reconstructed Lenna images.

Overall, the results indicate that all four denoising models can enhance an image to better correlate with the true, noiseless image. The performance increases with the number of iterations but begins to plateau at about 300 iterations.

The two tables show differences in performance. The ROF produces noticeably lower correlation coefficients. The Le model is marginally behind the AA model and the proposed model, in fact, the latter two models show practically the same performance.

Figures 4.1–4.4 give visual presentation of the enhanced pattern images, at varying number of iterations and using the different models. Figures 4.5–4.8 do the same for the Lenna image. Finally, Figures 4.9–4.13 present an actual ultrasound image and the enhanced images processed by each of the four variational models, at 100 iterations.
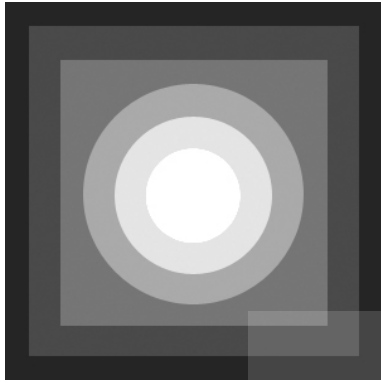
(a) Original pattern image.
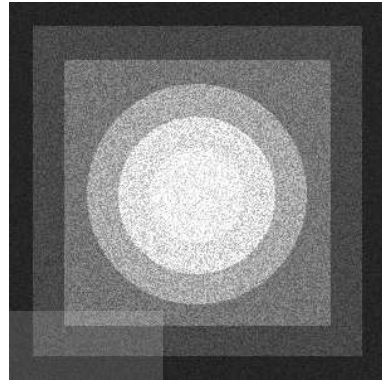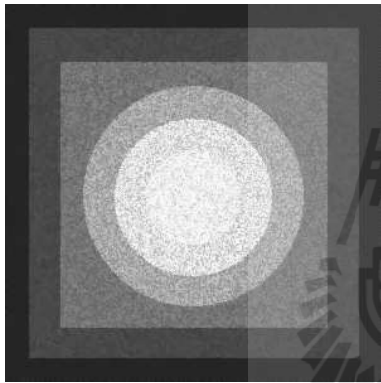
(b) Speckle noisy pattern image.

(c) image reconstructed by an 80-loops iterative process.
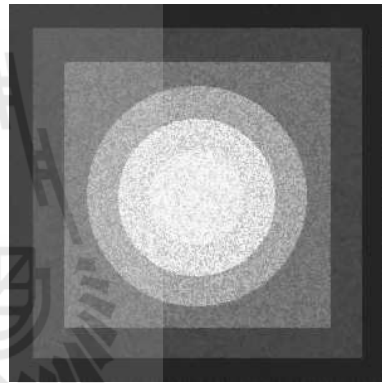
(d) image reconstructed by a 120-loops iterative process.
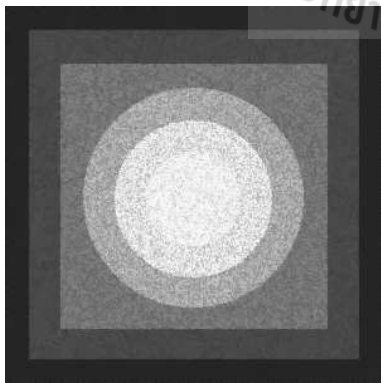
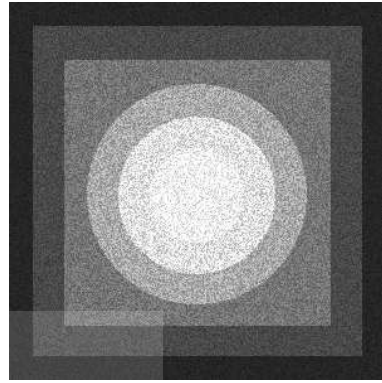(e) image reconstructed by a 160-loops iterative process.
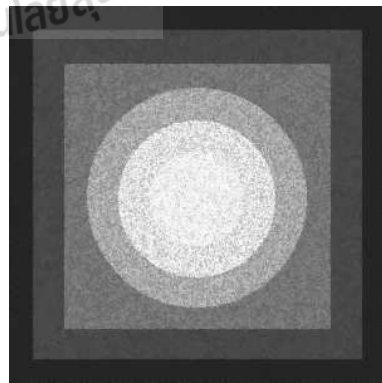
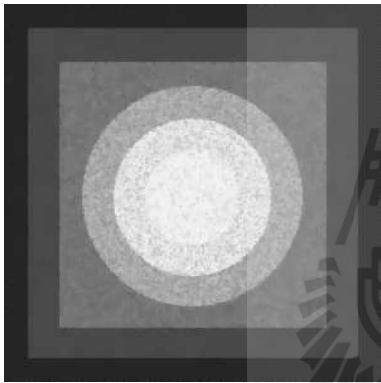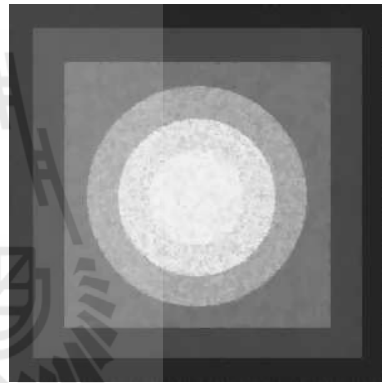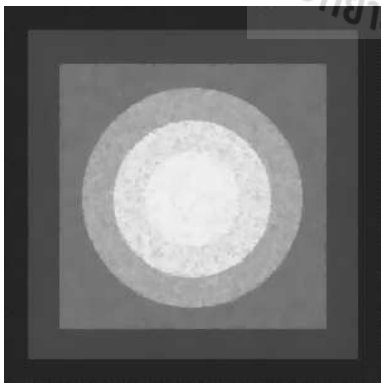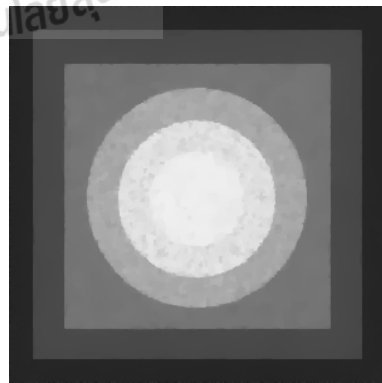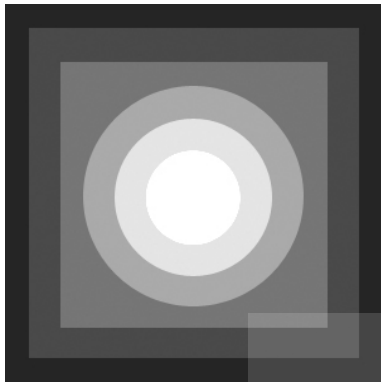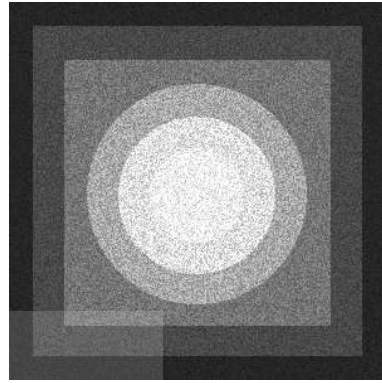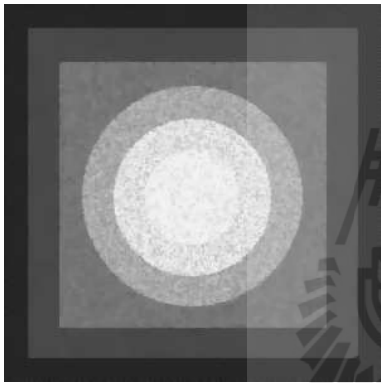(f) image reconstructed by a 200-loops iterative process.

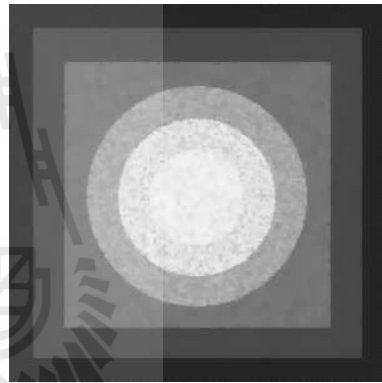Figure 4.1: The pattern image enhanced by the ROF model.
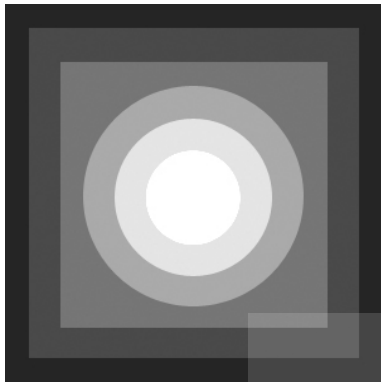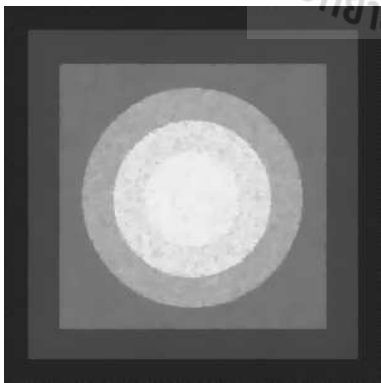
(a) Original pattern image.
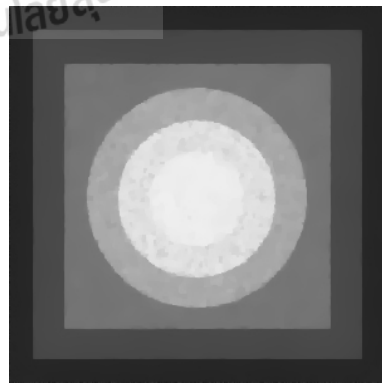
(b) Speckle noisy pattern image.

(c) image reconstructed by an 80-loops
iterative process.

(d) image reconstructed by a 120-loops
iterative process.

(e) image reconstructed by a 160-loops
iterative process.

(f) image reconstructed by a 200-loops
iterative process.

Figure 4.2: The pattern images enhanced by the Le model.

(a) Original pattern image.

(b) Speckle noisy pattern image.

(c) image reconstructed by an 80-loops iterative process.

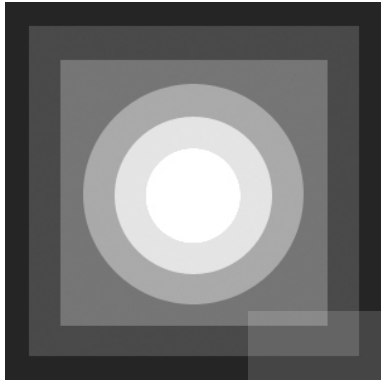(d) image reconstructed by a 120-loops iterative process.

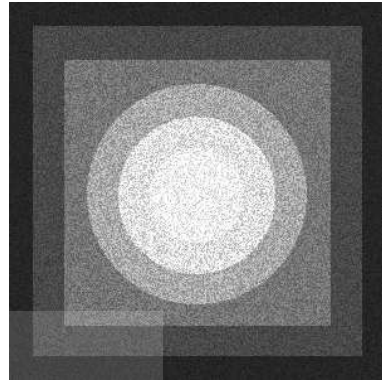(e) image reconstructed by a 160-loops iterative process.

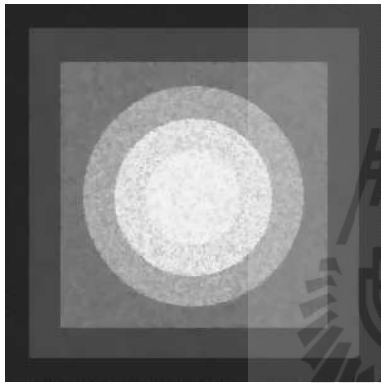(f) image reconstructed by a 200-loops iterative process.

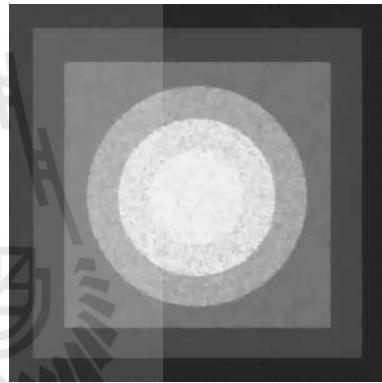Figure 4.3: The pattern image enhanced by the AA model.
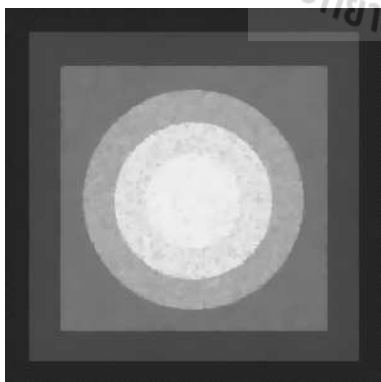
(a) Original pattern image.

(b) Speckle noisy pattern image.

(c) image reconstructed by an 80-loops iterative process.

(d) image reconstructed by a 120-loops iterative process.

(e) image reconstructed by a 160-loops iterative process.

(f) image reconstructed by a 200-loops iterative process.

Figure 4.4: The pattern image enhanced by the proposed model.

(a) Original Lenna image.

(b) Speckle noisy Lenna image.

(c) image reconstructed by a 40-loops iterative process.

(d) image reconstructed by a 60-loops iterative process.

(e) image reconstructed by an 80-loops iterative process.

(f) image reconstructed by a 100-loops iterative process.

Figure 4.5: The Lenna image enhanced by the ROF model.

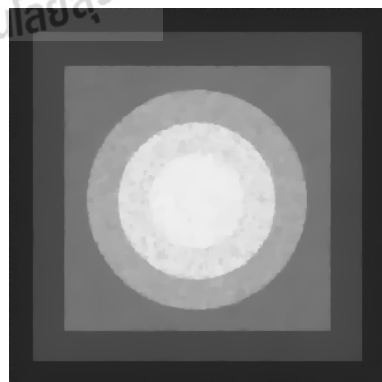(a) Original Lenna image.

(b) Speckle noisy Lenna image.

(c) image reconstructed by a 40-loops iterative process.

(d) image reconstructed by a 60-loops iterative process.

(e) image reconstructed by an 80-loops iterative process.

(f) image reconstructed by a 100-loops iterative process.

Figure 4.6: The Lenna image enhanced by the Le model.

(a) Original Lenna image.

(b) Speckle noisy Lenna image.

(c) image reconstructed by a 40-loops iterative process.

(d) image reconstructed by a 60-loops iterative process.

(e) image reconstructed by an 80-loops iterative process.

(f) image reconstructed by a 100-loops iterative process.

Figure 4.7: The Lenna image enhanced by the AA model.

(a) Original Lenna image.

(b) Speckle noisy Lenna image.

(c) image reconstructed by a 40-loops iterative process.

(d) image reconstructed by a 60-loops iterative process.

(e) image reconstructed by an 80-loops iterative process.

(f) image reconstructed by a 100-loops iterative process.

Figure 4.8: The Lenna image enhanced by the proposed model.

Figure 4.9: Original ultrasound image (Provided by Dr.Chumrus Sakulpaisarn).

Figure 4.10: Enhanced ultrasound image (ROF Model, 100 loops).

Figure 4.11: Enhanced ultrasound image (Le model, 100 loops).

Figure 4.12: Enhanced ultrasound image (AA model, 100 loops).

Figure 4.13: Enhanced ultrasound image (proposed model, 100 loops).

Chapter 5

Concluding Remarks

In this research work, a variational model for the reduction of ultrasound speckle noise was developed. The model is based on the assumption that the pixel intensity in an ultrasound image is Rayleigh distributed, caused by the uniformly distributed phases of the backscattered ultrasound waves and leading to significant image noise of multiplicative type. Then the existence and uniqueness of minimizers for the variational functional was discussed. Because of the multiplicative nature of the noise, the data fidelity term in the variational functional is no longer convex in general. Thus, while the existence of minimizers could be proved by applying compactness arguments, uniqueness required the additional assumption that brightness of the enhanced image at each pixel does not exceed that of the noisy image by a factor of $\sqrt{3}$. Finally, it was shown by means of numerical experiments that the proposed model can be applied to enhance image quality, and that it performs similarly or even better than some of the other variational models discussed in the literature.

The modeling of ultrasound speckle by the Rayleigh distribution is, however, relatively coarse. It is well conceivable that the Rician or the K-distributions should better match the appearance of speckle in ultrasound images. It therefore would be worthwhile to refine and adapt the model proposed here to these distributions in future work.

Bibliography

[1] G. Aubert and J.F. Aujol. (2008). A variational approach to remove multiplicative noise. **SIAM J. Appl. Math. (68)**(4):925–946.

[2] G. Aubert and P. Kornprobst. (2006). **Mathematical Problems in Image Processing: Partial Differential Equations and the Calculus of Variations**. 2nd ed., Springer.

[3] C.B. Burckhardt. (1978). Speckle in ultrasound B-mode scans. **IEEE Trans. Sonics and Ultrasonics. (25)**:1–6.

[4] A. Chambolle. (2004). An algorithm for total variation minimization and applications. **Interfaces Free Bound. (6)**:1–24.

[5] B. Dacorogna. (2004). **Introduction to the Calculus of Variations**. Imperial College Press.

[6] D.L. Donoho and I.M. Johnstone. (1994). Ideal spatial adaptation via wavelet shrinkage. **Biometrica**. **(81)**:425–455.

[7] L.C. Evans and R.F. Gariepy. (1992). **Measure Theory and Fine Properties of Functions**. CRC Press.

[8] V. Frost, J. Stiles, K. Shanmugan and J. Holzman. (1982). A model for radar images and its application to adaptive digital filtering and multiplicative noise. **IEEE Trans. PAMI**. **(4)**:157–166.

[9] J.W. Goodman. (1985). **Statistical Optics**. John Wiley & Sons.

[10] M.L. Green. (2002). **Statistics of Images, the TV Algorithm of Rudin-Osher-Fatemi for Image Denoising and an Improved Denoising Algorithm**. CAM Report, UCLA.

[11] M. Jansen. (2001). **Noise Reduction by Wavelet Thresholding**. Springer Verlag.

[12] J.A. Jensen. (1996). **Estimation of Blood Velocities Using Ultrasound: A Signal Processing Approach**. Cambridge University Press.

[13] P. Kornprobst, R. Deriche and G. Aubert. (1999). Image sequence analysis via partial differential equations. **J. Math. Imaging Vis. (11)**:5–26.

[14] K. Krissian, C.-F. Westin, R. Kikinis and K. Vosburgh. (2007). Oriented speckle reducing anisotropic diffusion. **IEEE Trans. Image Proc. (16)**:1412–1424.

[15] D.T. Kuan, A.A. Sawchuk, T.C. Strand and P. Chavel. (1985). Adaptive noise smoothing filter with signal-dependent noise. **IEEE Trans. PAMI**. **(7)**:165–177.

[16] T. Le, R. Chatrand and T.J. Asaki. (2007). A variational approach to reconstructing images corrupted by Poisson noise. **J. Math. Imaging Vis. (27)**:257–263.

[17] J. Lee. (1980). Digital image enhancement and noise filtering using local statistics, **IEEE Trans. PAMI**. **(2)**:165–168.

[18] P. Perona and J. Malik. (1990). Scale space and edge detection using anisotropic diffusion. **IEEE Trans. PAMI**. **(12)**:629–639.

[19] L.I. Rudin, S. Osher and E. Fatemi. (1992). Nonlinear total variation based noise removal algorithms. **Physica D**. **(60)**:259–268.

[20] W.R. Wade. (1999). **An Introduction to Analysis**, Prentice-Hall.

[21] Y. Yue, M.M. Croitoru, A. Bidani, J.B. Zwischenberger and J.W. Clark Jr. (2006). Nonlinear multiscale wavelet diffusion for speckle suppression and edge enhancement in ultrasound images. **IEEE Trans. Med. Imag. (25)**:297–311.
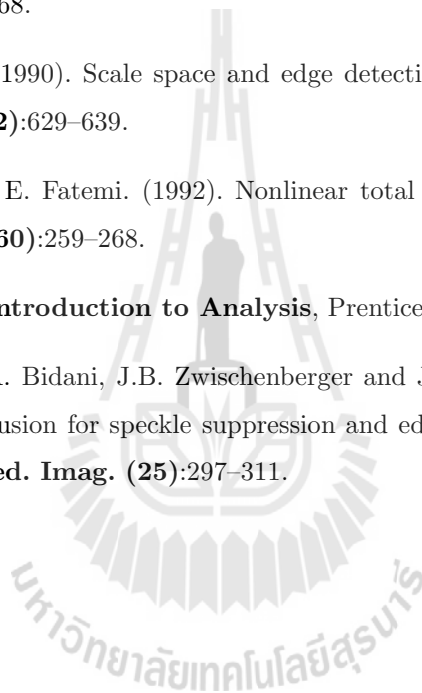
Curricula Vitae of Researchers

Name: Jessada Tanthanuch

Current Position: Assistant Professor, Suranaree University of Technology

Education: 2004   Ph.D. (Applied Mathematics),
Suranaree University of Technology, Thailand

               1997   B.Sc. (Mathematics, Second Class Honors),
Prince of Songkla University, Thailand

Professional Activities:

   2013 - current   Deputy Director, The Center for Educational Innovation and Technology, Suranaree University of Technology

   2004 - current   Assistant Professor in Mathematics, Suranaree University of Technology

Research Publications: (most recent)

1. J. Tanthanuch, W. Seekot and E. Schulz, *Ultrasound Image Enhancement by Means of a Variational Approach*, The Convergence of Imaging and Therapy Proceedings: 12th Asia-Oceania Congress of Medical Physics and 10th South East Asian Congress of Medical Physics, December 11-14, 2012, Chiang Mai, Thailand.

2. B. Nerysungnoen, K. Chompuvised and J. Tanthanuch, *Application of Mathematics for Noise Reduction and Edge Detection in Medical X-ray Image*, The Convergence of Imaging and Therapy Proceedings: 12th Asia-Oceania Congress of Medical Physics and 10th South East Asian Congress of Medical Physics, December 11-14, 2012, Chiang Mai, Thailand.

3. S. Rakkratok and J. Tanthanuch, *Solutions of Mathematics Problems Using Fibonacci Numbers and Examples by Spreadsheets*, ICEELT 2012 : International Conference on E-Education & Learning Technologies, August 13-14, 2012, Singapore.

4. J. Tanthanuch, *Symmetry Analysis of the nonhomogeneous inviscid Burgers equation with delay*, Communications in Nonlinear Science and Numerical Simulation. 17 (2012) 4978-4987.

5. S. Rakkratok, A. Hematulin and J. Tanthanuch, *Application of Fibonacci Numbers to Mathematical Problems*, ICER 2011 : Learning Communities for Sustainable Development, September 9-10, 2011, KKU, Thailand.

6. K. Dounjuntuk, T. Jittanan, P. Pradabsri and J. Tanthanuch, *Enrichment the High School Student Academic Achievement in Mathematics via the Project Approach Activity*, ICER 2011 : Learning Communities for Sustainable Development, September 9-10, 2011, KKU, Thailand.

7. P. Krissadeekorn T. Jittanan, P. Pradabsri and J. Tanthanuch, *The Mathematical Module of "Analytic Geometry" for Enrichment of High School Student Academic Achievements*, ICER 2011 : Learning Communities for Sustainable Development, September 9-10, 2011, KKU, Thailand.

8. T. Jittanan, P. Pradabsri, J. Tanthanuch, K. Khosonthongkee and S. Kupittayanant, *Network Development of Mathematics and Science Senior High School Education in Provincial Administrative Organization of Nakhon Ratchasima Schools*, ICER 2011 : Learning Communities for Sustainable Development, September 9-10, 2011, KKU, Thailand.

9. K. Thongrod, J. Tanthanuch, J. Angskun and T. Angskun, *The development of decision support system for oil transportation* (in Thai), ECTI-CARD 2010, May 10-12, Pattaya, Thailand, Mahanakorn University of Technology ISSN 978-974-8242-54-5.

10. J. Tanthanuch, *MPEG-Standard for Digital Movies and Sound* (in Thai), NCT Annual Review 2009, Vol.2/2 ISSN 1905-5870.

11. W. Seekot and J. Tanthanuch, *Ultrasound Image Enhancement by Means of a Variational Approach*, Proceedings of 11th National Graduate Research Conference, Graduate Studies: Sustainable Local Development, 17-18 December 2008,Graduate School, Valaya Alongkorn Rajabhat University, Pathum Thanni, Thailand.

12. J. Tanthanuch, *Mathematics in Telecommunication : From the Past to the Present* (in Thai), NCT Annual Review 2008, Vol.1/2 ISSN 1905-5870.

13. J. Tanthanuch, *Symmetry Analysis on* $\frac{\partial u}{\partial t}(x,t) + u(x,t)\frac{\partial u}{\partial x}(x,t) = G\big(u(x,t), u(x,t-\tau)\big)$, Proceedings of the 3rd IMT-GT Regional Conference on Mathematics, Statistics and Their Applications, 5-6 December 2007, Universiti Sains Malaysia, Penang, Malaysia, ISBN 978-983-3986-25-5.

14. S. Phosaard, J. Tanthanuch and J. PakPao, *3D: The Design and Implementation of a Three-Dimensional User Interface for an Operation System Using a Game Engine*, The 2007 International Conference of Applied and Engineering Mathematics (ICAEM), World Congress on Engineering 2007 (WCE 2007), London, U.K., 2-4 July, 2007.

15. J. Tanthanuch, *Symmetry Analysis on* $\frac{\partial u}{\partial t}(x,t) + u(x,t)\frac{\partial u}{\partial x}(x,t) = G\big(u(x,t-\tau)\big)$, Proceedings of the 2nd IMT-GT Regional Conference on Mathematics, Statistics and Their Applications. Vol. I - Pure Mathematics ISBN : 983-3391-86-9, 2006.

16. J. Tanthanuch, *"SOLITON" Mathematics for TSUNAMI* (in Thai), Thaksin Science Journal, Vol.2 No.1 (2005), 21-30.

17. J. Tanthanuch and S.V. Meleshko, *On definition of an admitted Lie group for functional differential equations.* Communications in Nonlinear Science and Numerical Simulation, 9 (2004), 117-125.

18. J. Tanthanuch, and S.V. Meleshko. *Application of group analysis to delay differential equations*, in: Nonlinear Acoustics at the Beginning of the 21st Century (2002), pp 607-610, Moscow, Russia: Faculty of Physics, Moscow State University.

Name: Eckart Schulz

Current Position: Assistant Professor, Suranaree University of Technology

Education: 1991   Ph.D. (Mathematics), University of Saskatchewan, Canada

               1985   M.Sc. (Mathematics), University of Saskatchewan, Canada

Professional Activities:

1993 - current   Asst. Prof. in Mathematics, Suranaree University of Technology

1995   Editor, AMC95 Conference Proceedings

1991 - 1993   Lecturer in Mathematics, Khon Kaen University

1990 - 1991   Lecturer in Mathematics, University of Saskatchewan, Canada

Research Publications: (most recent)

1. *Extensions of the Heisenberg group by one-parameter groups of dilations which are subgroups of the affine and the symplectic groups* (with K. Namngam), Math. Nachr. 288 (2015), 309-326.

2. *Equivalence of the metaplectic representation with sums of wavelet representations for a class of subgroups of the symplectic group* (with K. Namngam), J. Fourier Anal. 19 (2013), 77-114.

3. *Wavelet synthesis of continuous Brownian sheets* (with K. Nualtong), Int. J. Math. Anal. 6 (2012), 1763-1789.

4. *Linearization of second order stochastic differential equations* (with S.V. Meleshko), J. Nonlin. Math. Physics. 18 (2011), 427-441.

5. *Linearization of first order stochastic differential equations* (with S.V. Meleshko), Contributions in Mathematics and Applications III, East-West J. Math. Special volume, 2010, 178-186.

6. *A new set of admitted transformations for autonomous stochastic ordinary differential equations* (with S.V. Meleshko), J. Nonlin. Math. Physics. 17 (2010), pp. 179-196.

7. *On the definition of an admitted Lie group for stochastic differential equations* (with B. Srihirun, and S.V. Melesko), Commun. Nonlinear Sci. and Numer. Simul. 12 (2007), 1379-1389.

8. *On the definition of an admitted Lie group for stochastic differential equations with multi-Brownian motion* (with S.V. Meleshko, and B. Srihirun), J. Phys. A. 39 (2006), 13951-13966.

9. *Explicit cross sections of singly generated group actions* (with David Larson, Darrin Speegle and Keith F. Taylor), in: Harmonic Analysis and Applications (in honor of J. Benedetto), Christopher Heil editor, pp. 209-230, Birkhauser, 2006.

10. *Projections in L^1-algebras and Tight Frames* (with Keith F. Taylor), Contemporary Mathematics. 363 (2004), 313-319.

11. *Extensions of the Heisenberg Group and Wavelet Analysis in the Plane* (with Keith F. Taylor), CRM Lecture Notes and Conference Proceedings, 18(2000), 99-105.